Science of the Total Environment 768 (2021) 144796

Contents lists available at ScienceDirect

Science of the Total Environment

journal homepage: www.elsevier.com/locate/scitotenv

Enhanced atmospheric oxidation capacity and associated ozone increases during COVID-19 lockdown in the Yangtze River Delta

Yu Wang [a,1], Shengqiang Zhu [a,1], Jinlong Ma [a], Juanyong Shen [b], Pengfei Wang [c], Peng Wang [d,*], Hongliang Zhang [a,e,**]

[a] Department of Environmental Science and Engineering, Fudan University, Shanghai 200438, China
[b] School of Environmental Science and Engineering, Shanghai Jiao Tong University, Shanghai 200240, China
[c] Department of Civil and Environmental Engineering, Louisiana State University, Baton Rouge, LA 70803, USA
[d] Department of Civil and Environmental Engineering, Hong Kong Polytechnic University, Hong Kong 99907, China
[e] Institute of Eco-Chongming (IEC), Shanghai 200062, China

HIGHLIGHTS

- Enhanced atmospheric oxidation capacity is observed in the Yangtze River Delta during COVID-19 lockdown.
- NO_x reduction is the reason for increases of oxidants (OH, HO_2, and NO_3).
- O_3 is increased in the central Yangtze River Delta, corresponding to atmospheric oxidation capacity enhancement.

GRAPHICAL ABSTRACT

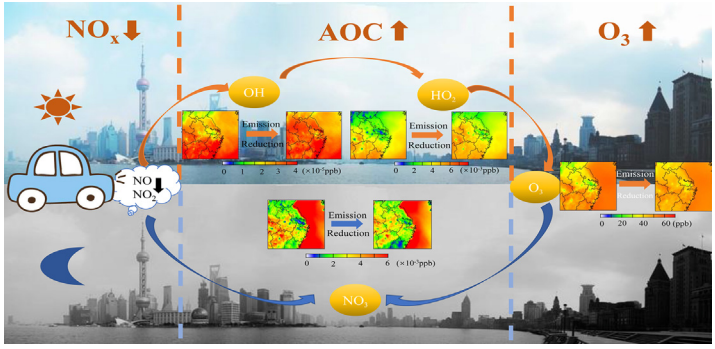

ARTICLE INFO

Article history:
Received 26 October 2020
Received in revised form 19 December 2020
Accepted 20 December 2020
Available online 7 January 2021

Editor: Pingqing Fu

Keywords:
COVID-19
Atmospheric oxidation capacity
Ozone
CMAQ
YRD

ABSTRACT

Aggressive air pollution control in China since 2013 has achieved sharp decreases in fine particulate matter ($PM_{2.5}$), along with increased ozone (O_3) concentrations. Due to the pandemic of coronavirus disease 2019 (COVID-19), China imposed nationwide restriction, leading to large reductions in economic activities and associated emissions. In particular, large decreases were found in nitrogen oxides (NO_x) emissions (>50%) from transportation. However, O_3 increased in the Yangtze River Delta (YRD), which cannot be fully explained by changes in NO_x and volatile organic compound (VOCs) emissions. In this study, the Community Multi-scale Air Quality model was used to investigate O_3 increase in the YRD. Our results show a significant increase of atmospheric oxidation capacity (AOC) indicated by enhanced oxidants levels (up to +25%) especially in southern Jiangsu, Shanghai and northern Zhejiang, inducing the elevated O_3 during lockdown. Moreover, net $P(HO_x)$ of 0.4 to 1.6 ppb h^{-1} during lockdown (Case 2) was larger than the case without lockdown (Case 1), mainly resulting in the enhanced AOC and higher O_3 production rate (+12%). This comprehensive analysis improves our understanding on AOC and associated O_3 formation, which helps to design effective strategies to control O_3.

1. Introduction

In recent decades, rapid economic growth significantly deteriorates air quality in China due to lack of emission controls (Hall et al., 2010; Zhao et al., 2012). In response, the Air Pollution Prevention and Control

* Corresponding author.
** Correspondence to: H. Zhang, Department of Environmental Science and Engineering, Fudan University, Shanghai 200438, China.
E-mail addresses: peng.ce.wang@polyu.edu.hk (P. Wang), zhanghl@fudan.edu.cn (H. Zhang).
[1] These authors contributed equally to this work.

https://doi.org/10.1016/j.scitotenv.2020.144796
0048-9697/

Action Plan was implemented in 2013 to improve air quality (Feng et al., 2019; Zheng et al., 2017). As fine particulate matter ($PM_{2.5}$) concentration is decreasing due to strict control measures (Geng et al., 2019; Zhang et al., 2018), ozone (O_3) concentration has an increasing trend (Chen et al., 2019; Wang et al., 2018), especially in populated and economically vibrant regions such as the Yangtze River Delta (YRD) (Ding et al., 2013; Shao et al., 2016; Xu et al., 2017). In recent years, the highest hourly O_3 frequently exceeded 160 $\mu g/m^3$ in the YRD (Li et al., 2019; Wang et al., 2019; Yang et al., 2020).

The sudden outbreak of the Coronavirus Disease 2019 (COVID-19) pandemic emerged significant social impacts in China (Atar and Atar, 2020; Nicola et al., 2020). To prevent the spread of COVID-19, a strict national lockdown was implemented since late January (Chinazzi et al., 2020; Tang et al., 2020). During the lockdown period, most transportation and commercial activities were terminated and almost all outdoor human activities were prohibited throughout the country, which gives an important opportunity to investigate the changes in air quality due to drastic emissions reduction. In the YRD, the alleviation of $PM_{2.5}$ was reported that attributed to the decrease in nitrogen oxides (NO_x) emissions (Bao and Zhang, 2020; Gautam, 2020; Ogen, 2020). However, elevated O_3 concentrations were observed in the YRD (Huang et al., 2020), indicating that challenges exist in O_3 control. The increase of O_3 is likely due to complex non-linear processes in O_3 formation and changes in atmospheric oxidation capacity (AOC) (Kentarchos and Roelofs, 2003; Li et al., 2015; Tan et al., 2019b). Thus, this is a need to investigate the change of AOC during COVID-19 outbreak and its relationship with O_3 increase to help establish more effective strategies in controlling $PM_{2.5}$ and O_3 synergistically.

AOC is defined as the sum of individual oxidation rates of primary pollutants (such as volatile organic compounds, VOCs) by oxidants including hydrogen oxide radicals ($HO_x = OH + HO_2$), and nitrogen oxide radical (NO_3) (Jacob, 2000; Monks, 2005; Singh et al., 1995). These oxidants are regarded as indicators to assess AOC, which determines characteristics of pollutants formation in the atmosphere (Geyer et al., 2001; Mao et al., 2010; Murray et al., 2014). In particular, hydroxyl radical (OH, major component of HO_x) plays important role in O_3 formation (Bloss et al., 2005; Sheehy et al., 2010). OH oxidizes VOCs to produce peroxy radicals, then peroxy radicals (such as HO_2) oxidize NO to produce NO_2 in competition with O_3 after NO_2 photolysis, leading to accumulation of O_3 (Fig. S1) (Pollack et al., 2013; Ren et al., 2013; Tan et al., 2019b).

Previous studies on AOC only focused on radical chemistry (Keywood et al., 2004; von Sonntag, 2007; Xue et al., 2016; Zheng et al., 2020). Limited studies have related to AOC changes with O_3 formation. Recent studies modeled the highest ever-reported concentrations of OH at urban site in the YRD (Zheng et al., 2020; Zhu et al., 2020), which indicates AOC is strong in this region. Therefore, it is necessary to study the changes of AOC due to NO_x emission and O_3 elevation during the COVID-19 lockdown period.

In this study, we use the Community Multiscale Air Quality (CMAQ) model to investigate AOC characteristics and associated O_3 changes in the YRD during the COVID-19 lockdown. Major oxidants and their sources are also determined and analyzed. The study aims to conduct an in-depth analysis on correlation of AOC and O_3 in the YRD with implications for formulating effective O_3 control policy in future.

2. Materials and methods

2.1. Model application

CMAQ version 5.0.2 with modified SAPRC-11 photochemical mechanism (Carter and Heo, 2013; Ying et al., 2015) was applied to simulate gas pollutants from January 5 to February 29, 2020 that comprises the pre-lockdown (January 5 to 22) and lockdown (January 23 to February 29) periods. Two-level nested domains were used with horizontal resolutions of 36-km and 12-km, respectively. The 36-km (197 × 127 grid cells) domain covered most of East Asia and the 12-km (97 × 88) domain included the YRD (Fig. S2). The Weather Research and Forecasting model (WRF) v3.6.1 was utilized to generate meteorology inputs to CMAQ with initial and boundary conditions from National Centers for Environmental Prediction (NCEP) FNL Operational Model Global Tropospheric Analyses dataset (NCEP, 2000; Zhang et al., 2012). The anthropogenic emissions were from Multi-resolution Emission Inventory for China (MEIC) for 2016 (http://www.meicmodel.org). Biogenic emissions were generated using the Model of Emissions of Gases and Aerosols from Nature v2.1 (Guenther et al., 2012).

2.2. Emission scenarios

Two simulation scenarios were performed in this study, with the business as usual case (Case 1) using unchanged emission and Case 2 adopting reduced emissions in the lockdown period. The decreases of emissions during lockdown were based on Huang et al. (2020). Provincial changes were made to carbon monoxide (CO, >13%), NO_x (>45%), sulfur dioxide (SO_2, >20%), VOCs (>30%), and PM (>15%). NO_2 levels declined the most during lockdown as transportation is the major source. Table 1 shows the detailed reduction ratios for each province in the YRD. By comparing the two cases, the impacts of reduced anthropogenic emissions on AOC and O_3 concentrations were evaluated.

2.3. Determining sources and sinks of oxidants

Quantifying contributions of individual processes to atmospheric oxidants provides a fundamental explanation and identifies key oxidants chemical characteristics related to AOC. Previous AOC studies have generally used box model to determine the sources and sinks of HO_x (Tan et al., 2017; Tan et al., 2019b; Zhu et al., 2020), which was constrained to observations of photolysis frequencies, long-lived trace gases, and meteorological parameters. And in this study, we used the CMAQ model. The process analysis technique in CMAQ was used, which includes integrated process rate (IPR) analysis and integrated reaction rate analysis (IRR) (https://www.cmascenter.org/cmaq/science_documentation/pdf/ch16.pdf) (Arshadi and Rajaram, 2015; Liu et al., 2010). The IRR analysis was directly computed from reaction rates at the beginning and end of each chemistry integration time step. Radical initiation reactions are almost always photolytic reactions that generate new radicals. The termination reactions remove radicals through the formation of stable products.

The budgets of HO_x including OH and HO_2 were evaluated quantitatively, aiming to identify the characteristics of AOC. In the radical production process, the major sources of OH and HO_2 are photolysis reactions involving nitrous acid (HONO), O_3, and formaldehyde (HCHO) and the reactions of O_3 with alkenes. In radical loss process, reactions that forms stable compounds such as $OH + NO_2 = HNO_3$ are considered. The detailed process of HO_x budget are shown in Table 2 that modified from Tan et al. (2019b). It should be noted that this study only considers chemical processes in the budget analysis, while physical processes such as deposition and transport are not included.

Table 1
Emission reduction factors for Case 2 during the lockdown period in this study. The scaling factors are from Huang et al. (2020).

Species	Province	NO_x	SO_2	VOC	PM	CO	BC	OC
Reduction factors	Shanghai	48%	42%	45%	34%	35%	54%	42%
	Jiangsu	50%	26%	41%	16%	23%	35%	7%
	Zhejiang	50%	29%	45%	30%	41%	49%	20%
	Anhui	56%	22%	31%	11%	14%	22%	4%
	Jiangxi	53%	21%	43%	19%	24%	30%	9%
	Fujian	51%	30%	42%	19%	29%	31%	7%
	Henan	57%	22%	41%	18%	23%	35%	8%
	Shandong	50%	25%	39%	19%	23%	35%	9%

Table 2
Chemical reactions considered in the radical budget analysis of OH and HO_2.

Product of HO_x		
HONO + hν	$HONO + h\nu\ (<400\ nm) \rightarrow OH + NO$	R1
$O^1D + H_2O$	$O(^1D) + H_2O \rightarrow OH + OH$	R2
HCHO + hν	$HCHO + h\nu\ (<335\ nm) + 2O_2 \rightarrow 2HO_2 + CO$	R3
O_3 + alkenes	$O_3 + alkenes \rightarrow OH, HO_2 + products$	R4
Loss of HO_x		
$OH + NO_2$	$OH + NO_2 \rightarrow HNO_3$	R5
$HO_2 + HO_2$	$HO_2 + HO_2 \rightarrow H_2O_2 + O_2$	R6
	$HO_2 + HO_2 + H_2O \rightarrow H_2O_2 + H_2O + O_2$	R7
$HO_2 + RO_2$	$HO_2 + RO_2 \rightarrow ROOH + O_2$	R8

2.4. O_3–NO_x–VOC sensitivity

The type of O_3 sensitivity regime is critical for the formation of O_3. Transition regime, NO_x-limited regime and VOC-limited regime have been demonstrated to explain the formation of O_3. At NO_x-limited regime (low NO conditions), VOCs are more competitive than NO_x to react with OH. The main reaction of VOCs and OH can produce peroxy radicals, leading to the O_3 concentration increase. At VOC-limited regimes (high NO conditions), the high levels NO can consume O_3 and suppress the accumulation of O_3 (named the "titration effect") (Chou et al., 2006). Here the ratio of R (define as $\frac{P_{H_2O_2}}{P_{HNO_3}}$) has been adopted to evaluate the O_3 production sensitivity, where $P_{H_2O_2}$ is the formation rate of hydrogen peroxide (H_2O_2), and P_{HNO_3} is the formation rate of nitric acid (HNO_3). And we take $R < 0.35$ as indicating VOC-limited regime, and $R > 0.35$ as NO_x-limited regime (Milford et al., 1994; Sillman et al., 1995). The spatial distributions of R reveal the characteristics of O_3 formation over the study area.

3. Results and discussions

3.1. WRF-CMAQ model validation

Meteorological conditions were validated against available observation data (~200 stations) from the National Climate Data Center (NCDC) (ftp://ftp.ncdc.noaa.gov/pub/data/noaa/isd-lite, last access August 2020) (Table S1). Temperature (T2) and wind speed (WS) were slightly overpredicted, indicating by positive mean bias (MB) values. MB values of wind direction was within benchmarks suggested by Emery and Tai (2001), while gross error (GE) values exceeded the benchmarks slightly. In general, WRF shows acceptable performance that is similar to previous studies over China (Hong et al., 2017; Hu et al., 2016; Hu et al., 2017).

CMAQ simulations were validated by comparing prediction with hourly observations from China National Environmental Monitoring Center (https://quotsoft.net/air, last access August 2020) (Table S2). Predicted O_3 (both O_3–1 h and O_3–8 h) and $PM_{2.5}$ were within the criteria suggested by US EPA with slightly overestimation (EPA, 2007). In three representative cities of YRD (Nanjing, Shanghai, and Hangzhou), predicted O_3 agreed well with observation, with MNB values of −0.03 to 0.01 (Fig. S3). The model performance is acceptable for NO_2 in Shanghai, while for Hangzhou and Nanjing, the model trend is the same, but there is a significant overestimation, which could be related to the inventory adjustment ratio in Zhejiang Province and Jiangsu Province (Fig. S4). Overall, CMAQ model gives robust results for following analysis.

3.2. Changes in AOC

3.2.1. Enhanced AOC in the YRD during the lockdown

During the COVID-19 lockdown, elevated AOC was predicted in Case 2 with emission reductions in large areas of the YRD, indicating by increased oxidants of OH, HO_2, and NO_3 (Fig. 1). Compared to Case 1, elevated OH and HO_2 in Case 2 occurred in most areas especially in Jiangsu, Shanghai and larger area of Zhejiang (Fig. 1c and f), with the growth rate of 15–20% and 10–25%, respectively. HO_x showed increases in similar regions (Fig. 1i) with less sink due to sharply reduced NO_x concentrations (Fig. S5c) (Atkinson et al., 2004; Jacob, 2000; Monks, 2005). Similarly, elevated NO_3 occurred in Jiangsu, Shanghai and northern Zhejiang (Fig. 1l) with highest increase of 17%, mainly due to reduced reactions with VOCs in HO_x and RO_2 production reactions ($NO_3 + alkenes = HO_x/RO_2 + products$, Fig. S6c) (Dentener and Crutzen, 1993; Fry et al., 2009; Rudich et al., 1998). NO_3 level showed a decrease by 15% in the southern Zhejiang during the lockdown, mainly due to declining O_3 and NO_2 (Fig. 4c and Fig. S5c) as the largest sources of NO_3 ($NO_2 + O_3 \rightarrow NO_3 + O_2$) (Brown and Stutz, 2012). Above all, the model captured AOC from pre-lockdown to lockdown over the YRD, with 10–25% elevations in Jiangsu, Shanghai and northern Zhejiang, and 2–10% declines in southern Zhejiang.

Averaged diurnal variations of major oxidants in three major cities (Nanjing, Shanghai and Hangzhou) are shown in Fig. 2. For HO_x, the peak values were observed at noontime, while, as the dominate oxidant in the nighttime, the higher levels of NO_3 occurred at the night. During the COVID-19 lockdown, elevated AOC was predicted in the Case 2 in three major cities, indicating by the rising major oxidants (OH, HO_2, and NO_3). Compared to Case 1, the daytime HO_x and nighttime NO_3 peak values were increased by 33–78% (50–78% in Nanjing, 33–50% in Shanghai, and 40–49% in Hangzhou) and 50–64% (50% in Nanjing and Hangzhou, and 64% in Shanghai), respectively. The HO_x peak value were the highest in Hangzhou (0.14 ppt for OH and 5.2 ppt for HO_2) in Case 2, followed by Nanjing (0.12 ppt for OH and 3.2 ppt for HO_2) and Shanghai (0.12 ppt for OH and 3 ppt for HO_2), which were consist with the average net $P(HO_x)$ for three major cities (-0.0688 ppb h^{-1} in Nanjing, -0.0602 ppb h^{-1} in Shanghai, and -0.0368 ppb h^{-1} in Hangzhou, see Sect 3.2.2). Similarly, the NO_3 peak value was the highest in Hangzhou (3.1 ppt) in Case 2, followed by Nanjing and Shanghai (2.2 ppt), demonstrating the higher AOC level in three major cities during the COVID-19 lockdown period especially in Hangzhou.

3.2.2. HO_x budget

Quantifying the production and loss rates of HO_x ($P(HO_x)$ and $L(HO_x)$) is crucial to understand the increase of AOC during the lockdown. The sources and sinks of HO_x in three major cities are shown in Fig. 3. From both Case 1 and Case 2, $P(HO_x)$ was dominated by photolysis reaction involving O_3, HONO, and HCHO. The photolysis of HONO (28%–52%, Table 2 R1), followed by HCHO (15%–25%, Table 2 R3) and O_3 (8%–20%, Table 2 R2) for the three cities in Case 1 (Fig. 3a–c). And the ozonolysis of alkenes (Table 2 R4) contributed 15%–29% during daytime and is the only primary source considered here at night. In addition, total $P(HO_x)$ declined in Case 2 compared to Case 1 (Fig. 3), which was mainly attributed to the lower $L(HO_x)$ rates. However, due to increase in O_3 concentrations (Fig. 4d–f), the enhanced ozonolysis of alkenes (0–0.2 ppb h^{-1}, Fig. S7) in all these cities were found in Case 2 at night. In Case 2, $P(HO_x)$ was dominated by photolysis of O_3 and HONO (both 25%–42%) and HONO (18%–35%) for the three cities. Also, in Case 2, the reaction of $O^1D + H_2O$ produced OH rates were up to 0.3 ppb h^{-1} in Shanghai at noontime, which is lower than that reported by Tan et al. (2019b) (1.4 ppb h^{-1}), due to the relatively low O_3 in winter (up to 56 ppb around noontime, Fig. 4d). In Shanghai, HCHO produced HO_2 rate was up to 0.2 ppb h^{-1} (Case 2), which was lower than previous studies (0.8 ppb h^{-1}) (Tan et al., 2019b; Zhu et al., 2020). The rates of HONO producing OH were (up to 0.2 ppb h^{-1} for Case 2) slightly lower than previous studies (up to 0.38 ppb h^{-1}) (Tan et al., 2019b; Wang et al., 2014; Zhu et al., 2020), which could be attributed to the absence of anthropogenic source emissions of HONO resulting in a lower HONO (Fig. S8). The ozonolysis of alkenes producing HO_x (~0.18 ppb h^{-1} averagely) are consistent with previous studies.

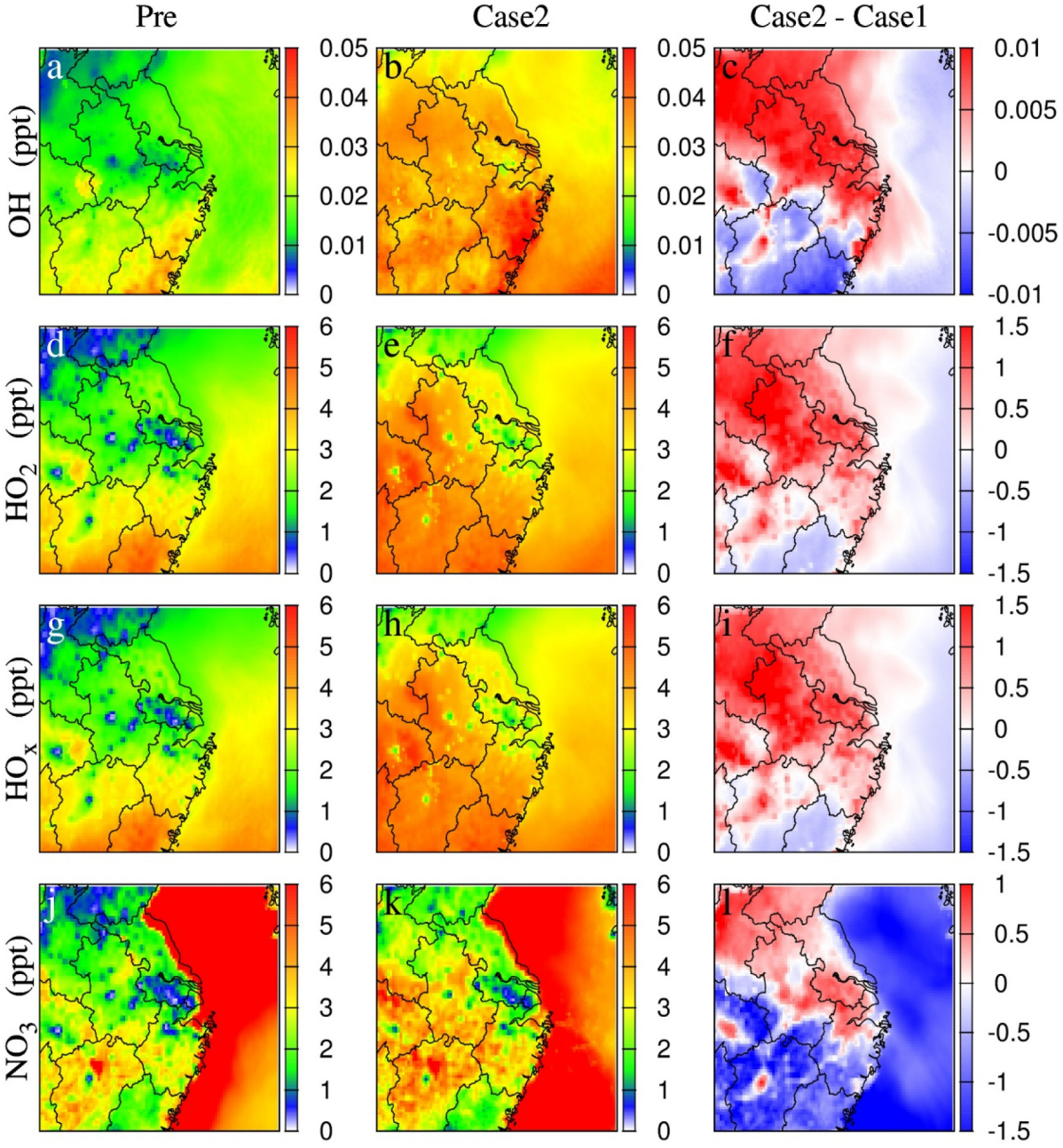

Fig. 1. Predicted the major oxidants and the changes between cases in unit of ppt during the pre-COVID (Pre) and COVID-lock periods (Case1 using unchanged emission and Case 2 adopting reduced emissions).

The lower L(HO_x) rates were found in Case 2 in all these cities, mainly due to a large decrease in NO_x (Fig. S5c) during the lockdown. From both Case 1 and Case 2, L(HO_x) was dominated by the reaction of OH + NO_2 (about 98%, Table 2 R5), followed by the reaction of HO_2 + HO_2 (2%, Table 2 R6). The HO_x losses via NO_x radical reactions were much larger than that of radical-radical reactions such as HO_2 + HO_2 (0.01–0.08 ppb h^{-1}, Table 2 R6-R8) for all the three cities, indicating a high-NO_x chemistry environment in the YRD. Consequently, total L(HO_x) declined significantly in Case 2 compared to Case 1 mainly due to the lower (30%–40%) NO_x emissions (Fig. S5). HO_x losses via NO_x–radical reactions were decreased 36% (up to 0.85 ppb h^{-1}), by 30% (up to 0.7 ppb h^{-1}), and 37% (up to 0.75 ppb h^{-1}) in Shanghai, Nanjing, and Hangzhou, respectively (Fig. S9).

As shown in Fig. S9, there was an imbalance between P(HO_x) and L (HO_x) rates (the net P(HO_x) = P(HO_x) - L(HO_x)) from both Case 1 and Case 2. Compared with Case 1, the net P(HO_x) was more significant in Case 2 ranging from −0.4 ppb h^{-1} to 1.6 ppb h^{-1}, mainly resulting in the enhanced AOC in the YRD during the lockdown. From the late afternoon until nighttime, the higher L(HO_x) (0.1 ppb h^{-1}) was observed compared to P(HO_x) from both cases. Similar uncertainties are also reported in Tan et al. (2019a), which could due to the exclusion of physical processes such as transport and depositions in the budget analysis.

3.3. Impacts of oxidants on O_3 formation

O_3 concentration during the lockdown was up to 12% higher in economically developed areas in comparison to Case 1, especially in southern Jiangsu, Shanghai and northern Zhejiang (Fig. 4a–c), consisting with elevated AOC in these areas. In major cities, the important increase in O_3 was found at noontime in Case 2, which is consistent with changes of

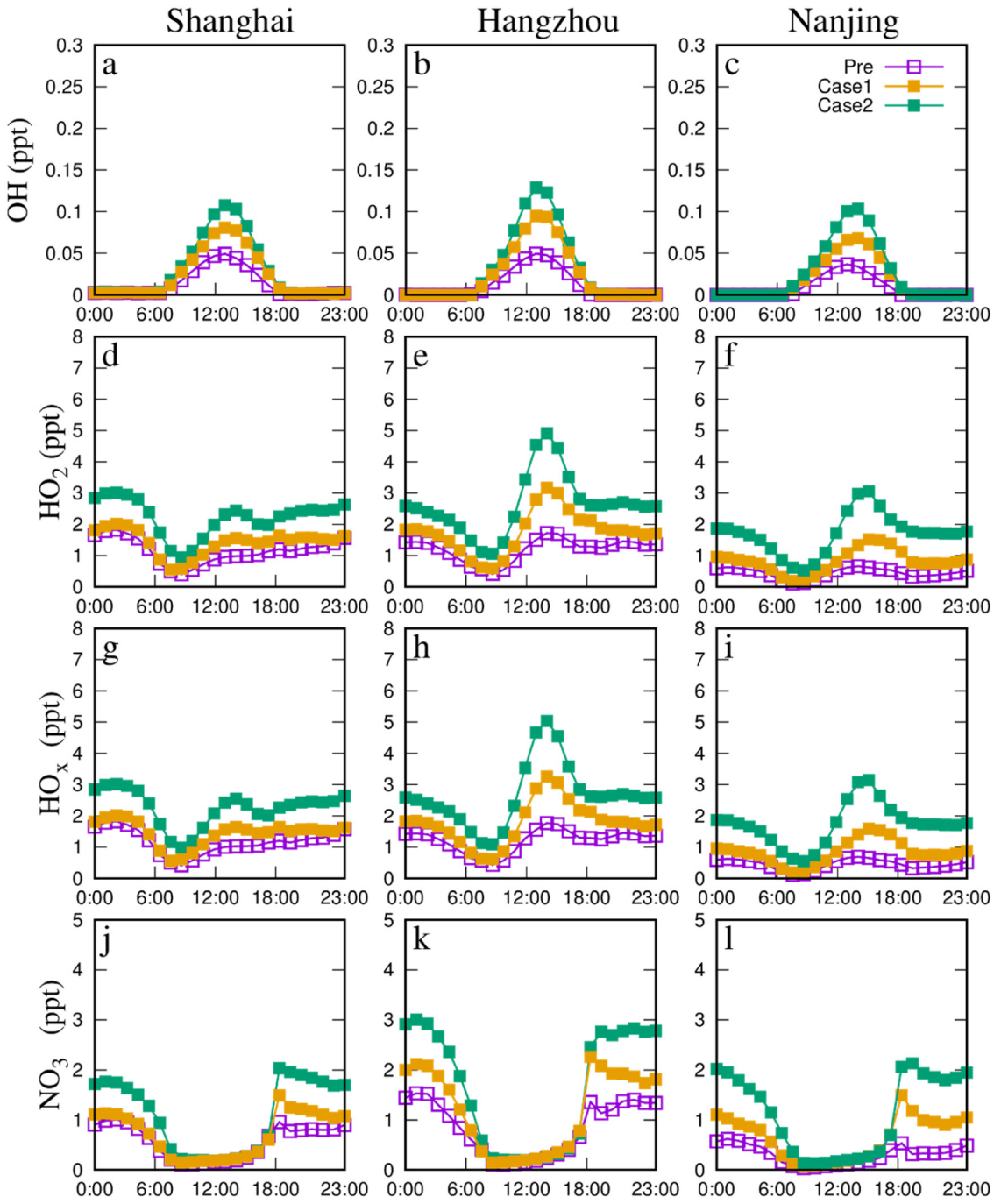

Fig. 2. Comparison of diurnal variation of predicted the major oxidants and the changes between cases in three major cities during the pre-COVID (purple squares represent Pre) and COVID-lock periods (yellow squares represent Case 1 in COVID-19 lockdown and green squares represent Case 2).

OH, the dominant oxidant (Fig. 4d–f). The diurnal variations of $P(HO_x)$ and $L(HO_x)$ further revealed the impacts of oxidants on O_3. In Case 2 the net $P(HO_x)$ was increased during nighttime (Fig. S7), implying that enhanced AOC increased O_3.

Meteorological conditions and changes in O_3 sensitivity regime could also be the reasons for O_3 increases (Sitnov, 1996; Tuck and Hovde, 1999; Wang et al., 2017a; Wang et al., 2017b; Wang et al., 2009). Further analysis was conducted to identify their roles. A slight increase in temperature during the lockdown period was observed (Fig. S10), which may play a role in increased O_3. Wind fields (Fig. S11) and relative humidity (Fig. S10) remained unchanged in comparison to pre-lockdown. As for O_3 sensitivity, the spatial distributions revealed the characteristics of O_3 formation over the YRD using an indicator (defined as $\frac{P_{H_2O_2}}{P_{HNO_3}}$) (Milford et al., 1994; Sillman et al., 1995). In the Case 1, VOC-limited regime mainly occurred in urban areas of Shanghai, southern Jiangsu, and Zhejiang, while NO_x-limited regime tended to be distributed over suburban areas. Compared to Case 1, Case 2 was indicative of noticeable changed from VOC-limited regimes to NO_x-limited regimes in eastern parts of Shanghai, southern Jiangsu, and northern Zhejiang (Fig. 4i). These areas were characterized by dramatical decline of NO_x emissions from mobile vehicles during the lockdown period, where O_3 increased significantly (Fig. 4c). The low levels NO_x can enhance AOC and further promote the accumulation of O_3 as discussed in section 3.2.1. VOC-limited regimes were mainly found in developed

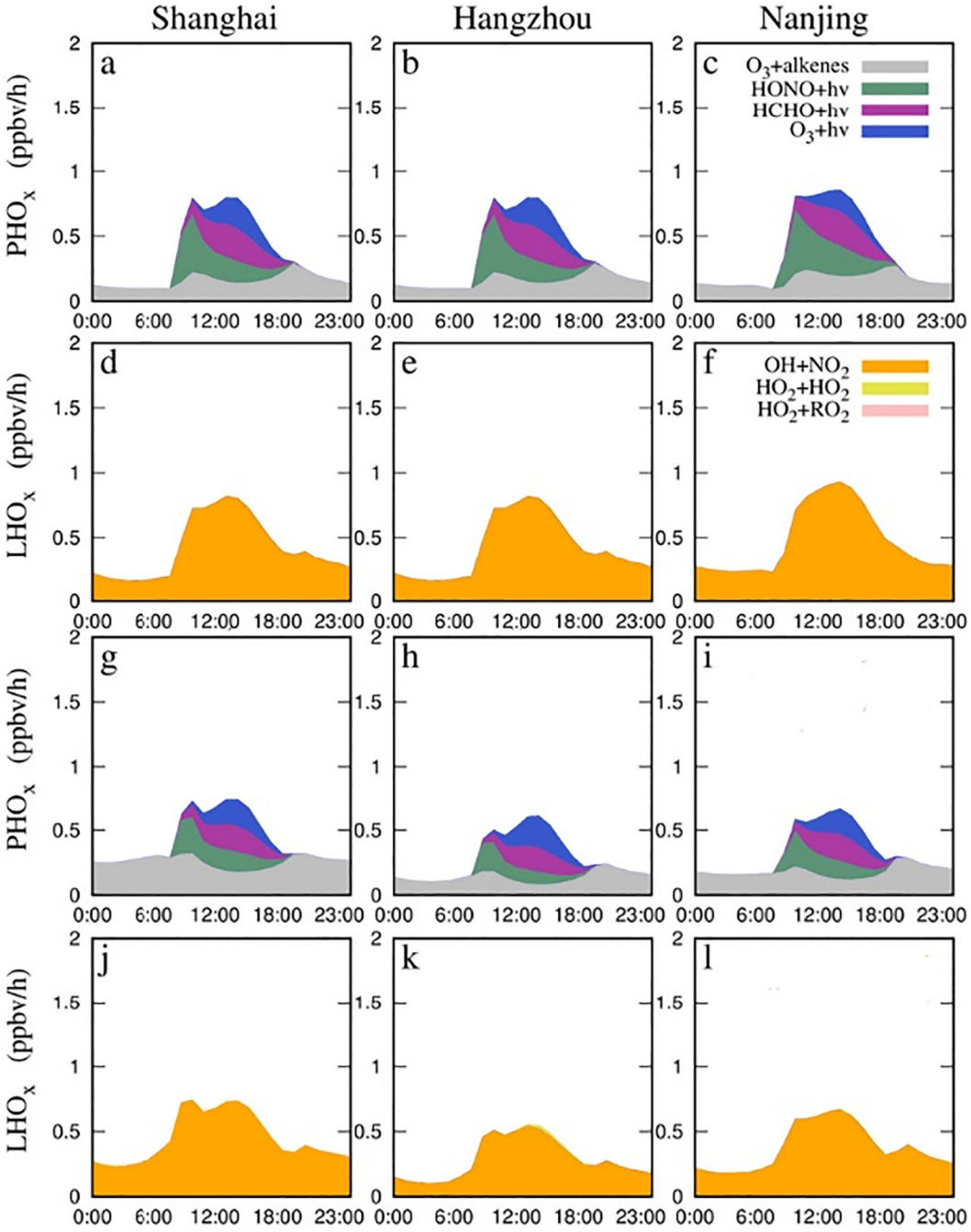

Fig. 3. Comparison of averaged diurnal variations of primary sources and sinks of HO_x radicals from model simulations (a-f) in Case 1 and (g-l) in Case 2 during the COVID-lock period.

urban regions such as most of southern Jiangsu in Case 2. In these regions (except for southern Zhejiang), the rising O_3 occurred during the lockdown, which is induced from the higher AOC in spite of the lower VOCs emissions. Therefore, elevated AOC can be deduced as the main contributor to elevated O_3 in YRD during the COVID-19 lockdown periods.

4. Conclusions

In this paper, oxidants and O_3 were simulated before and during the COVID-19 lockdown in the YRD using WRF/CMAQ modeling system with modified anthropogenic emissions. Results showed that the dramatic reductions in NO_x (>50%) led to up to 15–20%, 10–25%, and 17% increases of OH, HO_2, and NO_3 in Jiangsu, Shanghai, and northern Zhejiang during the lockdown period, respectively. Similarly, O_3 level was higher (up to 12%) in these regions during the lockdown period, consisting with changes of AOC. During the lockdown period, total P (HO_x) declined significantly in Case 2, compared with Case 1. In contrast, the ozonolysis of alkenes process increased at night (up to 0.2 ppb h^{-1}) due to increase in O_3 concentration. Total L(HO_x) declined significantly in Case 2, resulting from large reductions in NO_x emissions. The enhanced AOC was mainly attributed to the higher net P(HO_x) rates in the YRD. For three typical urban cities (Nanjing, Shanghai, and Hangzhou) in Case 2, P(HO_x) was dominated by photolysis of O_3 and HONO (both 25%–42%) and HONO (18%–35%). While the reaction of OH + NO_2 is the most important contributor to L(HO_x) (about 98%), followed by the reaction of HO_2 + HO_2.

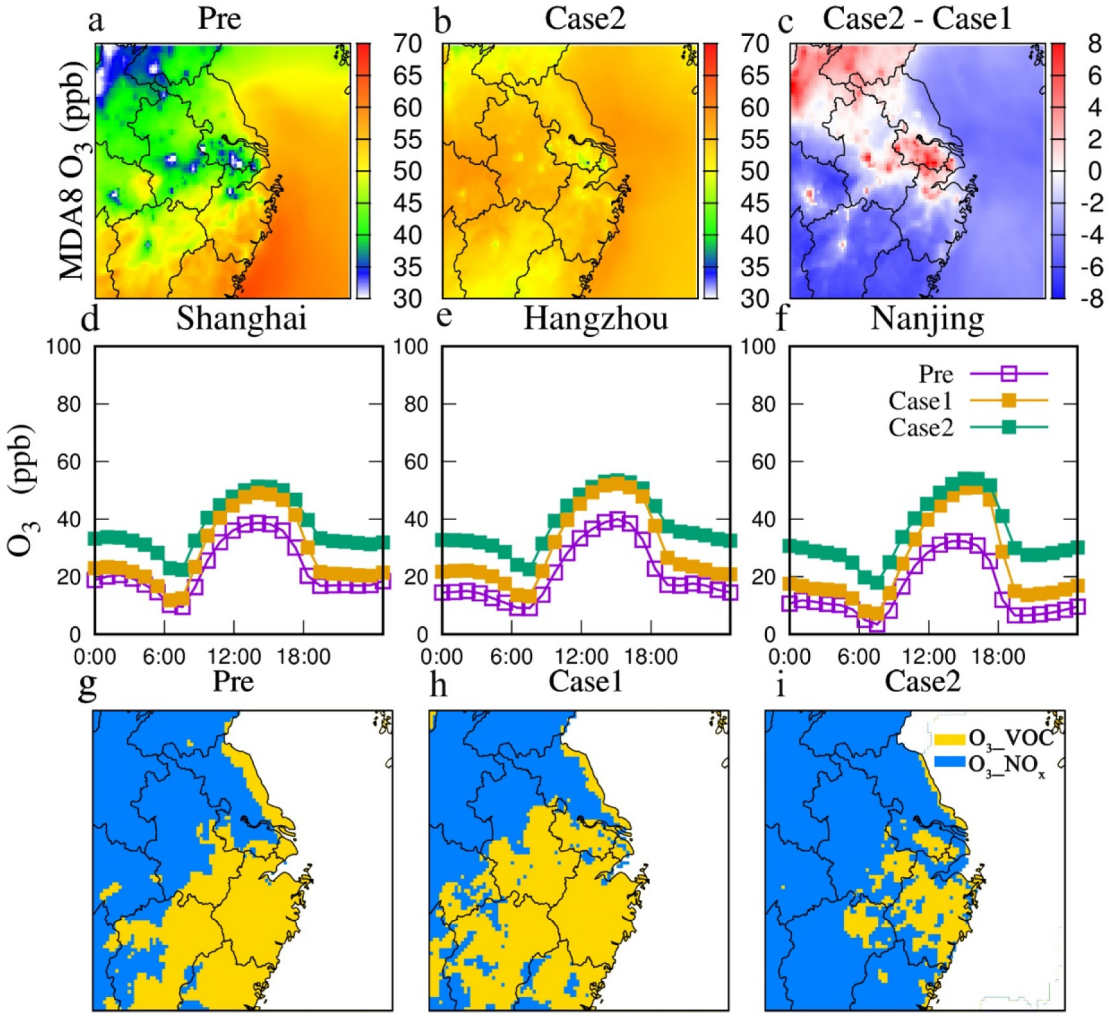

Fig. 4. (a–c) Spatial distribution of simulated MDA8 O_3 concentrations before and during COVID-19 lockdown period. (d–f) Averaged diurnal variations of modeled O_3 concentrations in three major cities (Purple squares represent the three weeks before COVID-19 outbreak, yellow squares represent Case 1 in COVID-19 lockdown, and green squares represent Case 2 in COVID-19 lockdown). (g–i) Spatial distributions of O_3 production sensitivity before and during COVID-19 lockdown.

Currently, O_3 pollution becomes the major air quality challenge in the YRD region while $PM_{2.5}$ concentrations has decreased in the recent decade. To mitigate O_3 pollution, more localized and stringent policies especially on controlling VOCs emissions should be implemented. This study also suggests the urgent need for a deep understanding of radical chemistry and AOC, so as to design more effective control strategies in the YRD.

CRediT authorship contribution statement

Yu Wang: Investigation, Visualization, Writing – original draft. **Shengqiang Zhu:** Methodology, Investigation, Writing – review & editing. **Jinlong Ma:** Methodology, Visualization. **Juanyong Shen:** Methodology, Investigation. **Pengfei Wang:** Investigation. **Peng Wang:** Methodology, Writing – review & editing. **Hongliang Zhang:** Conceptualization, Methodology, Writing – review & editing.

Declaration of competing interest

The authors declare that they have no conflict of interest.

Acknowledgments

This project was funded by Institute of Eco-Chongming (ECNU-IEC-202001). The data archiving is underway and will be uploaded to Mendeley Data.

Appendix A. Supplementary data

Supplementary data to this article can be found online at https://doi.org/10.1016/j.scitotenv.2020.144796.

References

Arshadi, M., Rajaram, H., 2015. A transition in the spatially integrated reaction rate of bimolecular reaction-diffusion systems. Water Resour. Res. 51, 7798–7810.

Atar, S., Atar, I., 2020. An invited commentary on "the socio-economic implications of the coronavirus and COVID-19 pandemic: a review". Int. J. Surg. 78, 122.

Atkinson, R., Baulch, D.L., Cox, R.A., Crowley, J.N., Hampson, R.F., Hynes, R.G., et al., 2004. Evaluated kinetic and photochemical data for atmospheric chemistry: volume I - gas phase reactions of O-x, HOx, NOx and SOx species. Atmos. Chem. Phys. 4, 1461–1738.

Bao, R., Zhang, A., 2020. Does lockdown reduce air pollution? Evidence from 44 cities in northern China. Sci. Total Environ. 731.

Bloss, W.J., Evans, M.J., Lee, J.D., Sommariva, R., Heard, D.E., Pilling, M.J., 2005. The oxidative capacity of the troposphere: coupling of field measurements of OH and a global chemistry transport model. Faraday Discuss. 130, 425–436.

Brown, S.S., Stutz, J., 2012. Nighttime radical observations and chemistry. Chem. Soc. Rev. 41, 6405–6447.

Carter, W.P.L., Heo, G., 2013. Development of revised SAPRC aromatics mechanisms. Atmos. Environ. 77, 404–414.

Chen, H., Zhuang, B., Liu, J., Wang, T., Li, S., Xie, M., et al., 2019. Characteristics of ozone and particles in the near-surface atmosphere in the urban area of the Yangtze River Delta, China. Atmos. Chem. Phys. 19, 4153–4175.

Chinazzi, M., Davis, J.T., Ajelli, M., Gioannini, C., Litvinova, M., Merler, S., et al., 2020. The effect of travel restrictions on the spread of the 2019 novel coronavirus (COVID-19) outbreak. Science 368 395−+.

Chou, C.C.K., Liu, S.C., Lin, C.Y., Shiu, C.J., Chang, K.H., 2006. The trend of surface ozone in Taipei, Taiwan, and its causes: implications for ozone control strategies. Atmos. Environ. 40, 3898–3908.
Dentener, F.J., Crutzen, P.J., 1993. Reaction of N2O5 on tropospheric aerosols - impact on the global distributions OF NOX, O3, and OH. J. Geophys. Res.-Atmos. 98, 7149–7163.
Ding, A.J., Fu, C.B., Yang, X.Q., Sun, J.N., Zheng, L.F., Xie, Y.N., et al., 2013. Ozone and fine particle in the western Yangtze River Delta: an overview of 1 yr data at the SORPES station. Atmos. Chem. Phys. 13, 5813–5830.
Emery, C., Tai, E., 2001. Enhanced Meteorological Modeling and Performance Evaluation for Two Texas Ozone Episodes.
EPA UEPA, Office of Air Quality Planning Standards. Guidance on the use of models and other analyses for demonstrating attainment of air quality goals for ozone, PM2. 5, and regional haze. 2007.
Feng, Y., Ning, M., Lei, Y., Sun, Y., Liu, W., Wang, J., 2019. Defending blue sky in China: effectiveness of the "air pollution prevention and control action plan" on air quality improvements from 2013 to 2017. J. Environ. Manag. 252.
Fry, J.L., Kiendler-Scharr, A., Rollins, A.W., Wooldridge, P.J., Brown, S.S., Fuchs, H., et al., 2009. Organic nitrate and secondary organic aerosol yield from NO3 oxidation of beta-pinene evaluated using a gas-phase kinetics/aerosol partitioning model. Atmos. Chem. Phys. 9, 1431–1449.
Gautam, S., 2020. COVID-19: air pollution remains low as people stay at home. Air Qual. Atmos. Health 13, 853–857.
Geng, G., Xiao, Q., Zheng, Y., Tong, D., Zhang, Y., Zhang, X., et al., 2019. Impact of China's air pollution prevention and control action plan on PM2.5 chemical composition over eastern China. Sci. China Ser. D Earth Sci. 62, 1872–1884.
Geyer, A., Alicke, B., Konrad, S., Schmitz, T., Stutz, J., Platt, U., 2001. Chemistry and oxidation capacity of the nitrate radical in the continental boundary layer near Berlin. J. Geophys. Res.-Atmos. 106, 8013–8025.
Guenther, A.B., Jiang, X., Heald, C.L., Sakulyanontvittaya, T., Duhl, T., Emmons, L.K., et al., 2012. The model of emissions of gases and Aerosols from nature version 2.1 (MEGAN2.1): an extended and updated framework for modeling biogenic emissions. Geosci. Model Dev. 5, 1471–1492.
Hall, J.V., Brajer, V., Lurmann, F.W., 2010. Air pollution, health and economic benefits-lessons from 20 years of analysis. Ecol. Econ. 69, 2590–2597.
Hong, C., Zhang, Q., Zhang, Y., Tang, Y., Tong, D., He, K., 2017. Multi-year downscaling application of two-way coupled WRF v3.4 and CMAQ v5.0.2 over East Asia for regional climate and air quality modeling: model evaluation and aerosol direct effects. Geosci. Model Dev. 10, 2447–2470.
Hu, J., Chen, J., Ying, Q., Zhang, H., 2016. One-year simulation of ozone and particulate matter in China using WRF/CMAQ modeling system. Atmos. Chem. Phys. 16, 10333–10350.
Hu, J., Li, X., Huang, L., Ying, Q., Zhang, Q., Zhao, B., et al., 2017. Ensemble prediction of air quality using the WRF/CMAQ model system for health effect studies in China. Atmos. Chem. Phys. 17, 13103–13118.
Huang, X., Ding, A., Gao, J., Zheng, B., Zhou, D., Qi, X., et al., 2020. Enhanced secondary pollution offset reduction of primary emissions during COVID-19 lockdown in China. Natl. Sci. Rev., nwaa137
Jacob, D.J., 2000. Heterogeneous chemistry and tropospheric ozone. Atmos. Environ. 34, 2131–2159.
Kentarchos, A.S., Roelofs, G.J., 2003. A model study of stratospheric ozone in the troposphere and its contribution to tropospheric OH formation. J. Geophys. Res.-Atmos. 108.
Keywood, M.D., Kroll, J.H., Varutbangkul, V., Bahreini, R., Flagan, R.C., Seinfeld, J.H., 2004. Secondary organic aerosol formation from cyclohexene ozonolysis: effect of OH scavenger and the role of radical chemistry. Environ. Sci. Technol. 38, 3343–3350.
Li, H., Li, L., Huang, C., J-y, An, R-s, Yan, H-y, Huang, et al., 2015. Ozone source apportionment at urban area during a typical photochemical pollution episode in the Sumner of 2013 in the Yangtze River Delta. Huanjing Kexue 36, 1–10.
Li, L., An, J., Huang, L., Yan, R., Huang, C., Yarwood, G., 2019. Ozone source apportionment over the Yangtze River Delta region, China: investigation of regional transport, sectoral contributions and seasonal differences. Atmos. Environ. 202, 269–280.
Liu, X.-H., Zhang, Y., Xing, J., Zhang, Q., Wang, K., Streets, D.G., et al., 2010. Understanding of regional air pollution over China using CMAQ, part II. Process analysis and sensitivity of ozone and particulate matter to precursor emissions. Atmos. Environ. 44, 3719–3727.
Mao, J., Ren, X., Chen, S., Brune, W.H., Chen, Z., Martinez, M., et al., 2010. Atmospheric oxidation capacity in the summer of Houston 2006: comparison with summer measurements in other metropolitan studies. Atmos. Environ. 44, 4107–4115.
Milford, J.B., Gao, D.F., Sillman, S., Blossey, P., Russell, A.G., 1994. Total reactive nitrogen (no(y)) as an indicator of the sensitivity of ozone to reductions in hydrocarbon and NOX emissions. J. Geophys. Res.-Atmos. 99, 3533–3542.
Monks, P.S., 2005. Gas-phase radical chemistry in the troposphere. Chem. Soc. Rev. 34, 376–395.
Murray, L.T., Mickley, L.J., Kaplan, J.O., Sofen, E.D., Pfeiffer, M., Alexander, B., 2014. Factors controlling variability in the oxidative capacity of the troposphere since the last glacial maximum. Atmos. Chem. Phys. 14, 3589–3622.
NCEP F. National Centers for Environmental Prediction/National Weather Service/NOAA/US Department of Commerce, 2000. Updated daily. Research data archive at the National Center for Atmospheric Research, Computational and Information Systems Laboratory. 2000.
Nicola, M., Alsafi, Z., Sohrabi, C., Kerwan, A., Al-Jabir, A., Iosifidis, C., et al., 2020. The socio-economic implications of the coronavirus pandemic (COVID-19): a review. Int. J. Surg. 78, 185–193.
Ogen, Y., 2020. Assessing nitrogen dioxide (NO2) levels as a contributing factor to coronavirus (COVID-19) fatality. Sci. Total Environ. 726.
Pollack, I.B., Ryerson, T.B., Trainer, M., Neuman, J.A., Roberts, J.M., Parrish, D.D., 2013. Trends in ozone, its precursors, and related secondary oxidation products in Los Angeles, California: a synthesis of measurements from 1960 to 2010. J. Geophys. Res.-Atmos. 118, 5893–5911.
Ren, X., van Duin, D., Cazorla, M., Chen, S., Mao, J., Zhang, L., et al., 2013. Atmospheric oxidation chemistry and ozone production: results from SHARP 2009 in Houston, Texas. J. Geophys. Res.-Atmos. 118, 5770–5780.
Rudich, Y., Talukdar, R.K., Ravishankara, A.R., 1998. Multiphase chemistry of NO3 in the remote troposphere. J. Geophys. Res.-Atmos. 103, 16133–16143.
Shao, P., An, J., Xin, J., Wu, F., Wang, J., Ji, D., et al., 2016. Source apportionment of VOCs and the contribution to photochemical ozone formation during summer in the typical industrial area in the Yangtze River Delta, China. Atmos. Res. 176, 64–74.
Sheehy, P.M., Volkamer, R., Molina, L.T., Molina, M.J., 2010. Oxidative capacity of the Mexico City atmosphere - part 2: a ROx radical cycling perspective. Atmos. Chem. Phys. 10, 6993–7008.
Sillman, S., THE USE, OF NOY, 1995. H2O2, and HNO3 as indicators for ozone-NOX-hydrocarbon sensitivity in URBAN locations. J. Geophys. Res.-Atmos. 100, 14175–14188.
Singh HB, Kanakidou M, Crutzen PJ, Jacob DJ. HIGH-CONCENTRATIONS AND PHOTOCHEMICAL FATE OF OXYGENATED HYDROCARBONS IN THE GLOBAL TROPOSPHERE. Nature 1995; 378: 50–54.
Sitnov, S.A., 1996. Vertical structure of the extratropical quasi-biennial oscillation in ozone, temperature, and wind derived from ozonesonde data. J. Geophys. Res.-Atmos. 101, 12855–12866.
Tan, Z., Fuchs, H., Lu, K., Hofzumahaus, A., Bohn, B., Broch, S., et al., 2017. Radical chemistry at a rural site (Wangdu) in the North China plain: observation and model calculations of OH, HO2 and RO2 radicals. Atmos. Chem. Phys. 17, 663–690.
Tan, Z., Lu, K., Hofzumahaus, A., Fuchs, H., Bohn, B., Holland, F., et al., 2019a. Experimental budgets of OH, HO2, and RO2 radicals and implications for ozone formation in the Pearl River Delta in China 2014. Atmos. Chem. Phys. 19, 7129–7150.
Tan, Z., Lu, K., Jiang, M., Su, R., Wang, H., Lou, S., et al., 2019b. Daytime atmospheric oxidation capacity in four Chinese megacities during the photochemically polluted season: a case study based on box model simulation. Atmos. Chem. Phys. 19, 3493–3513.
Tang, B., Wang, X., Li, Q., Bragazzi, N.L., Tang, S., Xiao, Y., et al., 2020. Estimation of the transmission risk of the 2019-nCoV and its implication for public health interventions. J. Clin. Med. 9.
Tuck, A.F., Hovde, S.J., 1999. Fractal behavior of ozone, wind and temperature in the lower stratosphere. Geophys. Res. Lett. 26, 1271–1274.
von Sonntag, C., 2007. The basics of oxidants in water treatment. Part a: OH radical reactions. Water Sci. Technol. 55, 19–23.
Wang, X., Chen, F., Wu, Z., Zhang, M., Tewari, M., Guenther, A., et al., 2009. Impacts of weather conditions modified by urban expansion on surface ozone: comparison between the Pearl River Delta and Yangtze River Delta regions. 26, 962–972.
Wang, F., An, J., Li, Y., Tang, Y., Lin, J., Qu, Y., et al., 2014. Impacts of uncertainty in AVOC emissions on the summer ROx budget and ozone production rate in the three most rapidly-developing economic growth regions of China. Adv. Atmos. Sci. 31, 1331–1342.
Wang, T., Xue, L., Brimblecombe, P., Lam, Y.F., Li, L., Zhang, L., 2017. Ozone pollution in China: a review of concentrations, meteorological influences, chemical precursors, and effects. Sci. Total Environ. 575, 1582–1596.
Wang, J., An, J., Shao, P., Zou, J., Lin, X., Zhang, YjHjkxHk, 2017a. Characteristic study on the" weekend effect" of atmospheric O3 in Northern Suburb of Nanjing. 38, 2256–2263.
Wang, Y., Du, H., Xu, Y., Lu, D., Wang, X., Guo, Z., 2018. Temporal and spatial variation relationship and influence factors on surface urban heat island and ozone pollution in the Yangtze River Delta, China. Sci. Total Environ. 631-632, 921–933.
Wang, N., Lyu, X., Deng, X., Huang, X., Jiang, F., Ding, A., 2019. Aggravating O-3 pollution due to NOx emission control in eastern China. Sci. Total Environ. 677, 732–744.
Xu, Z., Huang, X., Nie, W., Chi, X., Xu, Z., Zheng, L., et al., 2017. Influence of synoptic condition and holiday effects on VOCs and ozone production in the Yangtze River Delta region, China. Atmos. Environ. 168, 112–124.
Xue, L., Gu, R., Wang, T., Wang, X., Saunders, S., Blake, D., et al., 2016. Oxidative capacity and radical chemistry in the polluted atmosphere of Hong Kong and Pearl River Delta region: analysis of a severe photochemical smog episode. Atmos. Chem. Phys. 16, 9891–9903.
Yang, G., Liu, Y., Li, X., 2020. Spatiotemporal distribution of ground-level ozone in China at a city level. Sci. Rep. 10, 7229.
Ying, Q., Li, J., Kota, S.H., 2015. Significant contributions of isoprene to summertime secondary organic aerosol in eastern United States. Environ. Sci. Technol. 49, 7834–7842.
Zhang, H., Li, J., Ying, Q., Yu, J.Z., Wu, D., Cheng, Y., et al., 2012. Source apportionment of PM2.5 nitrate and sulfate in China using a source-oriented chemical transport model. Atmos. Environ. 62, 228–242.
Zhang, N.-N., Ma, F., Qin, C.-B., Li, Y.-F., 2018. Spatiotemporal trends in PM2.5 levels from 2013 to 2017 and regional demarcations for joint prevention and control of atmospheric pollution in China. Chemosphere 210, 1176–1184.
Zhao, J., Chen, S., Wang, H., Ren, Y., Du, K., Xu, W., et al., 2012. Quantifying the impacts of socio-economic factors on air quality in Chinese cities from 2000 to 2009. Environ. Pollut. 167, 148–154.
Zheng, Y., Xue, T., Zhang, Q., Geng, G., Tong, D., Li, X., et al., 2017. Air quality improvements and health benefits from China's clean air action since 2013. Environ. Res. Lett. 12.
Zheng, J., Shi, X.W., Ma, Y., Ren, X.R., Jabbour, H., Diao, Y.W., et al., 2020. Contribution of nitrous acid to the atmospheric oxidation capacity in an industrial zone in the Yangtze River Delta region of China. Atmos. Chem. Phys. 20, 5457–5475.
Zhu, J., Wang, S., Wang, H., Jing, S., Lou, S., Saiz-Lopez, A., et al., 2020. Observationally constrained modeling of atmospheric oxidation capacity and photochemical reactivity in Shanghai, China. Atmos. Chem. Phys. 20, 1217–1232.